Journal of Nano- and Electronic Physics
Vol. **17** No 3, 03022(5pp) (2025)

Журнал нано- та електронної фізики
Том **17** № 3, 03022(5cc) (2025)

OPEN ACCESS

REGULAR ARTICLE

DFT Performance Analysis of Graphene Nanoribbon FET with Gate Stack for Low Power Applications

Ritam Dutta[1,*], Debmitra Das[2]

[1] *Dept. of CSE (IoT), Poornima Institute of Engineering & Technology, Jaipur, India*
[2] *Dept. of CSE, Poornima University, Jaipur, India*

(Received 05 April 2025; revised manuscript received 18 June 2025; published online 27 June 2025)

This article presents the improved device performance of graphene nanoribbon field effect transistor with novel structure. In this proposed structure, number of carbon atoms are varied along armchair graphene nanoribbon (AGN) width (n), across the channel. The channel material is developed with gate stack approach. Moreover, the carrier transport using huckel extended (HE) model-based density functional theory (DFT) is studied. The rise in the value of 'n' from 4 to 8 in the channel material enhances the ON current (I_{ON}), reduces OFF current (I_{OFF}), improves the switching ratio, and reduces threshold voltage (V_{th}) 29 %, results reduced drain induced barrier lowering (DIBL) in A8 device (GS-GNFET with AGN (n = 8) in channel material) as compared with A4 device having (GS-GNFET with AGN (n = 8) in channel material). The device density of states (DDOS) analysis confirms higher electron occupation and better performance of A8 device compared to A4 device model. The tight-binding Hamiltonian matrix is solved using the HE model and a semi-empirical calculator. A 33 % improvement in ON current and a 76 % reduction in OFF current have been recorded in our proposed GS-GNFET device model over conventional GNRFET. Moreover, the A8 device has a very low value of static power (1.69×10^{-13} watt) compared to pre-established experimental data recorded through literature survey.

Keywords: AGN, GS-GNFET, DIBL, DFT, DDOS, TP.

DOI: 10.21272/jnep.17(3).03022 PACS numbers: 81.05.ue, 85.30.Pq

1. INTRODUCTION

With the advent of nanotechnology, the development of graphene material as nanoribbon in field-effect transistors presents a remarkable roadmap in developing modern physics-based electronics where silicon-based technology is challenged [1]. With its revolutionary finding in 2004, graphene, a single atom-thick sheet of carbon arranged in a hexagonal lattice, captivated researchers' interest. Its excellent electrical, mechanical, and thermal characteristics suggest its potential for various uses, including transistors. In its purest form, graphene is essentially a semimetal with no bandgap, making it difficult to switch on and off as necessary for transistor applications [2]. There must be an existence of tunable bandgap of graphene that can make it suitable in transistor applications. Several methods have been employed to induce a bandgap, including transforming graphene into thin graphene strips named graphene nanoribbons (GNRs) [3].

Moreover, based on edge scaling, these nanoribbons are classified into two main categories: armchair graphene nanoribbons (AGN) and zigzag graphene nanoribbons (ZGN) [4]. The edges in the AGN are of armchair type, while in ZGNRs, the edges are of zigzag type.

AGN based model shows metallic behavior. The semiconducting behavior of AGN having n = 3p and 3p + 1 makes it suitable to use as a channel material in nanoscale-based transistors. Furthermore, the gate oxide of the transistor must be chosen from substances possessing a high dielectric constant to enhance its functionality and decrease the short channel effects (SCEs) in the nanoscale-based transistors [5]. However, the process of directly depositing high-κ dielectrics on AGN based substrate seems to be exciting task for researchers [6]. To overcome this challenge, a gate stack architecture (GS) can be employed, where a thin passivation layer (SiO_2 layer) between the AGN substrate and high-κ dielectrics, keeping the oxide thickness constant [7].

2. PROPOSED DEVICE STRUCTURE

Our proposed device structure is designed with Lanthanum Aluminate ($LaAlO_3$ Layer) nanoparticle-based layer which is insulated through Silicon Di-Oxide (SiO_2 Layer) layer over the channel. In addition to this, to reduce SCE effect, the gate stack is employed below metal gate (G), shown in Fig. 1. The AGN with n = 4 and n = 8 is used as channel material.

The device model is further simulated keeping typical device parameters with calibrated values mentioned in Table 1, where calibrated physical and electrical parameters used for simulation process is shown.

* Correspondence e-mail: ritamdutta1986@gmail.com

Cite this article as: R. Dutta et al., *J. Nano- Electron. Phys.* 17 No 3, 03022 (2025) https://doi.org/10.21272/jnep.17(3).03022

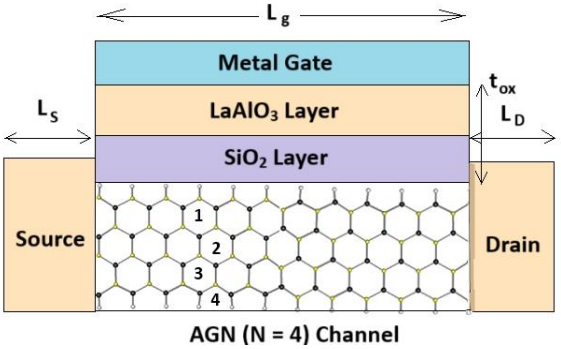

Fig. 1 – Proposed device model

Table 1 – Physical & Electrical parameters used in this model

Device Parameters	Proposed Devices	
	A4 Device	A8 Device
Gate Length (L_g) in nm	7 to 10	7 to10
Length of Source (L_S) and Drain (L_D)	5 nm	5 nm
Oxide Thickness (t_{ox}) in nm	0.5 to 2	0.5 to 2
Doping at source (N_s) in atoms/cm^3	4.5×10^{16}	4.5×10^{16}
Doping at drain (N_d) in atoms/cm^3	1.5×10^{14}	1.5×10^{14}
Doping at intrinsic channel (N_{ch}) in atoms/cm^3	4×10^{12}	4×10^{12}
Supply Voltage (V_{DD})	0.5 V	0.5 V

3. PROCESS METHODOLOGY

This section presents the simulation methodology in step-by-step manner. All the simulations are carried out in TCAD software. The tight-binding Hamiltonian matrix approach with the HE model is employed in the semi-empirical calculator. The value of density mesh cut-off is taken as 40 Hartree (Ha), and K-point sampling is taken as 100 along the C-direction. The summarized process flow chart for the simulation approach is displayed in Fig. 2.

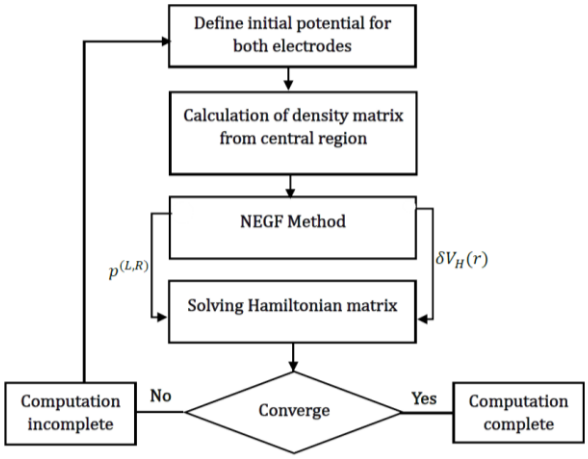

Fig. 2 – Flow chart of the simulation process

The density matrix for the central region in the device can be calculated as [9]:

$$D(V_b) = \int_{-\infty}^{\infty} [p^L(\in, V_b) n_F(\in -\mu_L) + p^R(\in, V_b) n_F(\in -\mu_R)] d\epsilon \quad (1)$$

Where, p^L – partial spectral density of states (DOS) in the left electrode

p^R – partial spectral DOS in the right electrode

V_b – external bias voltage

μ_L – the chemical potential of the left electrode

μ_R – the chemical potential of the right electrode

The partial spectral densities with Non-Equilibrium Green's Function (NEGF) method are given as [10]:

$$p^{L,R\ (\varepsilon,\ V_b)} = \frac{1}{2\pi} [G(\varepsilon, V_b)\, \Gamma^{L,R}(\varepsilon) G^{\dagger}(\varepsilon, V_b) \quad (2)$$

Where, $p^{(L,\ R)}$ – spectral densities of states in left and right electrodes

G – Green's function

$\Gamma^{(L,\ R)}$ – Broadening function

$G^{\dagger}$ – Advanced Green's function

From the density matrix and partial spectral densities, the real-space density for the central region is calculated, which is given as [11]:

$$\delta n(r) = \sum \delta m_u \sqrt{\frac{a_u}{\pi}}\, e^{-\alpha_u |r - R_u|^2} \quad (3)$$

Where, m_u – Mulliken population

α_u – width of the Gaussian orbital

After calculating real space density matrix, the Hartree potential is calculated by solving Poisson's equations using the HE-SCF method. The Hartree potential is given by [12]:

$$-\nabla . [\varepsilon(r) \nabla\, \delta V_H(r)] = \delta n(r) \quad (4)$$

Where,

$\varepsilon(r)$ – spatially dependent dielectric constant

$\delta V_H(r)$ – Hartree potential

$\delta n(r)$ – Induced electron density

Now, Hartree potential is used to solve the one-electron Hamiltonian until a self-consistent solution is gained. The one-electron Hamiltonian can be calculated as [13]:

$$H_{ij} = E_i + \delta V_H(R_i) \quad if\ i = j$$
$$H_{ij} = \frac{1}{4} (\beta_i + \beta_j)(E_i + E_j) S_{ij} + \frac{1}{2} [(\delta V_H(R_i) + \delta V_H(R_j) S_{ij})] \quad if\ i \neq j \quad (5)$$

Where,

H_{ij} – One-electron Hamiltonian

E_i – Orbital energy

β_i – Adjustable parameter

$\delta V_H(R_i)$ – Hartree potential corresponds to the induced electron density on the atoms

As the self-consistent solution of the tight-binding Hamiltonian matrix from Eq. (6) is obtained, the transmission coefficient T(E) and drain current are calculated. The transmission coefficient is given as [14]:

$$T(E) = Trace[G(E) \Gamma_d(E) G^{\dagger} \Gamma_s(E)] \quad (6)$$

Where,

$T(E)$ – transmission coefficient

$G(E)$ – retarded Green's function

$G^{\dagger}(E)$ – advanced Green's function

$\Gamma_d(E)$ – broadening function of the left electrode

$\Gamma_s(E)$ – broadening function of the right electrode

4. SIMULATION RESULTS

In this section, firstly the *V*/*I* characteristics of the proposed GS-GNFET is compared with a pre-established experimental data collected from recent survey. Furthermore, the effect of varying '*n*' values in the bulk configuration of AGN is investigated in terms of bandgap, DOS, and *T*(*E*). Moreover, these bulk-configured AGNs with different '*n*' values are employed in channel material, and the performance of both proposed devices is compared in terms of DFT parameters for low-power applications.

In Fig. 3, the *V*/*I* characteristics is compared between the pre-established experimental data with our proposed simulated model. The simulation model is calibrated with fixed device dimensions (L_g = 7 to 10 nm, t_{ox} = 0.5 to 2 nm) and AGN (N = 8) material in the entire channel region. The Schrodinger equation is solved using the NEGF method and a self-consistent tight binding function to derive the device characteristics for the proposed model. It is evident from the simulation, that our simulated model is having very similar plot compared with the pre-established dataset.

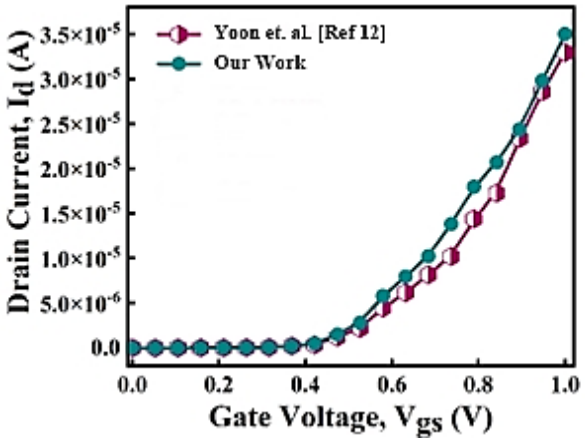

Fig. 3 – *V*/*I* characteristics comparison

Fig. 4 describes the transfer characteristics comparison between our proposed GS-GNFET with conventional GNFET keeping all device physical and electrical parameters constant. In Fig. 4, the left side depicts the logarithmic change in drain current (I_d) with gate voltage (V_{gs}), whereas the right side shows the linear change of I_d with V_{gs}. The logarithmic scale of I_d with V_{gs} illustrates the leakage current (I_{OFF}) in the device, that further provides an insight about variation of subthreshold slope.

On the other hand, the linear relationship between I_d and V_{gs} provides the threshold voltage (V_{th}). The OFF current in case of our proposed GS-GNFET device model decreased from 8.62×10^{-11} to 3.15×10^{-12} A, and the on-current increased from 6.18×10^{-6} to 8.44×10^{-6} A. In our proposed device, the I_{OFF} is reduced by 76 %, and the I_{ON} is improved by 33 %. The results show that the GS-GNFET records better results over conventional GNRFET device.

Fig. 5 (a) and 5 (b) shows the energy band gap (EBD) analysis of bulk-configured AGNs for different values of n = 4 and 8 using HE model. The band gap, which displays the total number of possible energy levels for an electron, is calculated using band structure shown below.

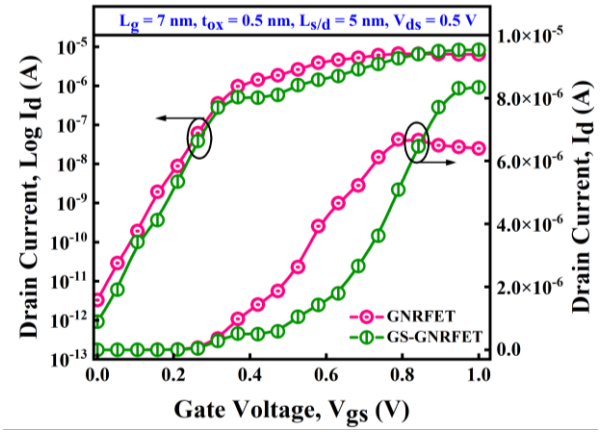

Fig. 4 – *V*/*I* characteristics of GNRFET and proposed GS-GNFET

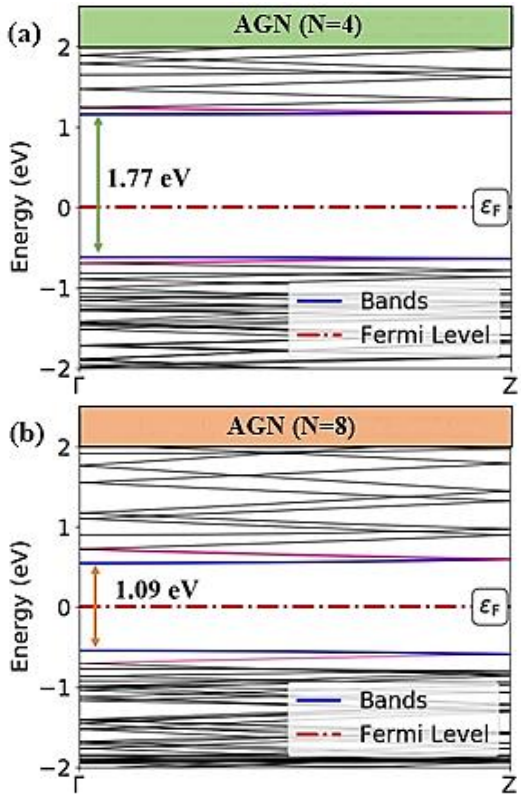

Fig. 5 – EBD Analysis of AGN with (a) N = 4, and (b) N = 8 band structure

The density of states (DOS) denotes the number of states that are accessible in the energy range E and $E + dE$ within volume (V). A higher DOS value signifies the availability of greater states for occupation. The DOS can be calculated as [13]:

$$D(E) = \frac{N(E)}{dE} \quad (7)$$

Where,
$D(E)$ – DOS the available energy range
$N(E)$ – Number of available states in the range dE having energy (E)

Now, the higher value of DIBL signifies a lesser control of the gate over the channel, which leads to higher

power consumption and degradation in device performance. therefore, the DIBL is calculated as [14]:

$$DIBL = \frac{V_{th}(at\ high V_{ds}) - V_{th}(at\ low\ V_{ds})}{V_{ds}(High) - V_{ds}(low)} \quad (8)$$

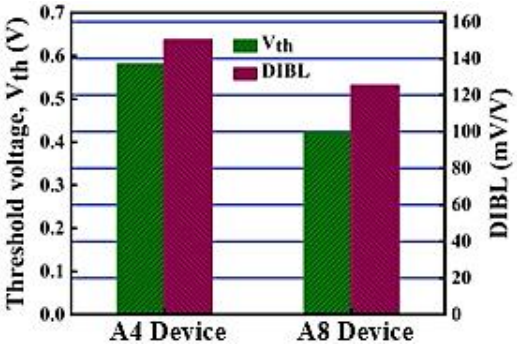

Fig. 6 – DIBL comparison between A4 and A8 devices

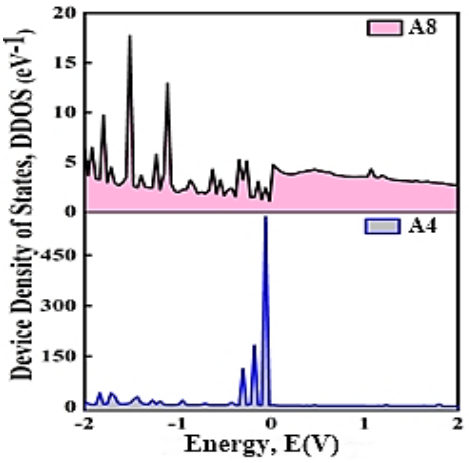

Fig. 7 – DDOS vs Energy comparison between A4, A8 devices

In Fig. 6 the bar graph comparison between the A4 and A8 device is well established, that shows A8 device has got lesser value of DIBL, which signifies lower power consumption over the A4 device. The value of DIBL reduces from 150 to 122 mV/V for A8 device. The reason is that the A8 device has a smaller bandgap, lower threshold voltage, and better switching speed, which improves the control of the gate over the channel and reduces DIBL value as compared with the A4 device.

Fig. 7 depicts the variation of DDOS in both A4 and A8 devices. The DDOS presents the total number of electronic states that are obtainable, how they are distributed in terms of energy.

5. CONCLUSION

Finally, it can be concluded that the performance of our proposed GS-GNFET with gate stack architecture provides better device performance compared to orthodox GNRFET devices. The tight-binding Hamiltonian matrix is solved using the HE model and a semi-empirical calculator. A 33 % improvement in ON current and a 76 % reduction in OFF current have been recorded in our proposed GS-GNFET device model over conventional GNRFET.

Furthermore, the effect of varied '*n*' on the performance of GS-GNFET is thoroughly studied. The rise in the value of '*n*' from 4 to 8 improves I_{ON} by 511 times, reduces I_{OFF} by 99.83 %, improves the switching ratio, reduces V_{th} by 29 %, and reduces DIBL by 18 % in the A8 device as compared to A4 device.

Besides this, transport properties viz. DDOS are studied to analyze the performance of both devices. The analysis of DDOS concludes that the A8 device exhibits a greater area under the curve in both the valence and conduction bands, indicating a higher electron occupation and better overall device performance.

REFERENCES

1. A. Anshul, R. Chaujar, R.P. Reimann, *Int. Conf. on Recent Trends Microelectronics, Automation, Comp. Commun. Sys.* **88** (2022).
2. T. Radsar, H. Khalesi, V. Ghods, *Superlattice. Microstruct.* **153**, 106869 (2021).
3. E. Kan, Z. Li, J. Yang, *Phys. Appl. Graphene-theory* **10**, 14112 (2011).
4. A. Hazra, S. Basu, *C – J. Carbon Res.* **4** No 3, 49 (2021).
5. B. Kumar, M. Sharma, *Microelectron. J.* **135**, 105766 (2023).
6. T. Marmolejo, J.V. Medina, *Microelectron. J.* **48**, 18 (2016).
7. B.H. Lee, J. Oh, H. Tseng, R. Jammy, *Mater. Today* **9**, 32 (2006).
8. B. Kumar, M. Sharma, *Microelectron. J.* **139**, 105910 (2023).
9. T.N. Todorov, J. Hoekstra, A. Sutton, *Philosophical Magazine B* **80**, 421 (2020).
10. K. Stokbro, D. Petersen, S. Smidstrup, A. Blom, *Phys. Rev. B* **82**, 075420 (2010).
11. M. Whangbo, R. Hoffmann, *J. Chem. Phys.* **68**, 5498 (1978).
12. S. Smidstrup, T. Markussen, P. Vancraeyveld, *J. Phys.: Condens. Matter.* **32**, 015901 (2019).
13. R. Jyoti, M. Chowhan, *ES Energy Environ.* **18**, 47 (2022).
14. A. Anshul, R. Chaujar, *IEEE Trans. Nanotechnol.* **23**, 400 (2024).

Аналіз продуктивності DFT на основі графенових нанострічкових польових транзисторів зі стеком затворів для застосувань з низьким енергоспоживанням

Ritam Dutta[1], Debmitra Das[2]

[1] *Dept. of CSE (IoT), Poornima Institute of Engineering & Technology, Jaipur, India*
[2] *Dept. of CSE, Poornima University, Jaipur, India*

У цій статті представлено покращені характеристики польового транзистора на основі графенової нанострічки з новою структурою. У запропонованій структурі кількість атомів вуглецю змінюється вздовж ширини (n) крісельної графенової нанострічки (AGN) поперек каналу. Матеріал каналу розроблено з використанням підходу стеку затворів. Крім того, досліджується транспорт носіїв заряду з використанням розширеної моделі Хюккеля (HE) на основі теорії функціоналу густини (DFT). Збільшення значення 'n' від 4 до 8 у матеріалі каналу збільшує струм увімкнення (I_{ON}), зменшує струм вимкнення (I_{OFF}), покращує коефіцієнт перемикання та зменшує порогову напругу (V_{th}) на 29 %, що призводить до зменшення зниження бар'єру, індукованого стоком (DIBL) у пристрої A8 (GS-GNFET з AGN (n = 8) у матеріалі каналу) порівняно з пристроєм A4, що має (GS-GNFET з AGN (n = 8) у матеріалі каналу). Аналіз густини станів пристрою (DDOS) підтверджує вищу зайнятість електронів та кращу продуктивність пристрою A8 порівняно з моделлю пристрою A4. Матрицю гамільтоніана з щільним зв'язком розв'язують за допомогою моделі HE та напівемпіричного калькулятора. У запропонованій нами моделі пристрою GS-GNFET було зафіксовано покращення струму ввімкнення на 33 % та зменшення струму вимкнення на 76 % порівняно зі звичайним GNRFET. Більше того, пристрій A8 має дуже низьке значення статичної потужності ($1{,}69 \times 10^{-13}$ Вт) порівняно з попередньо встановленими експериментальними даними, отриманими з огляду літератури.

Ключові слова: AGN, GS-GNFET, DIBL, DFT, DDOS, TP.